EurJIC
European Journal of Inorganic Chemistry

Research Article
doi.org/10.1002/ejic.202400260

Chemistry Europe
European Chemical Societies Publishing

www.eurjic.org

VIP *Very Important Paper*

Hydrogen Bonding vs Dihydrogen Bonding in the Air Stable Primary Phosphine *ortho*-Phosphinophenol

Alexander M. Stone,[a] Andrew R. Golden,[a] Shan M. Daniel,[a] Arnold L. Rheingold,[b] and John D. Protasiewicz*[a]

This article is dedicated to Professor Rainer Streubel, an inspirational pioneer of novel phosphorus compounds.

ortho-Phosphinophenol (**oPP**) is an unusual example of an air-stable primary phosphine and a valuable precursor to a variety of useful organophosphorus compounds. The presence of PH_2 and OH functionalities offers the possibility of intermolecular and intramolecular P···HO hydrogen bonding (**HB**). The close proximity of these two groups also offers the opportunity for intramolecular PH_2···HO dihydrogen bonding (**DHB**). This work provides experimental and computational evidence for these various types of interactions. In the solid state, **oPP** is associated by significant intermolecular P···HO hydrogen bonds as revealed by a single crystal X-ray structural determination. Multinuclear NMR and IR spectroscopic studies, coupled with DFT computational studies, suggest that **oPP** adopts multiple conformations in solution whose nature varies with the identity of the solvent. In the gas phase or non-polar solvents (such as cyclohexane) an equilibrium between four conformations of **oPP** is proposed. Interestingly, *in silico*, a conformational isomer having bifurcated intramolecular PH_2···HO **DHB** (**PP4**) is found to be more stable than a conformational isomer having intramolecular P···HO **HB** (**PP1**). In polar solvents (**S**), NMR studies indicate intermolecular OH···**S HB** plays a dominant role in modulating ^{31}P NMR chemical shifts over a 17 ppm range.

Introduction

Hydrogen bonding (**HB**) is a key feature in determining secondary structures within and between molecules, with impacts across diverse fields such as biology, chemistry, and material science.[1–3] While weaker than covalent bonds, the presence of hydrogen bonds is ubiquitous in nature, and the impacts of such forces scale with the number of hydrogen bonds. Conventional hydrogen bonding involves a combination of (a) electrostatic interactions between H and A atoms and (b) bonding interactions involving donation of electron density from lone pair electrons on the hydrogen bond acceptor (A) with a σ* orbital of the hydrogen bond donor (X–H) to form an X–H···A array (Scheme 1, left). Linear X–H···A geometries afford maximum interaction. This interplay between these two interactions has been described as electrostatics being the engine and the orbital interactions the steering wheel.[4] Typically X is an electronegative atom (such as N, O, S, or F) having a polarized X–H bond which enhances the positive charge on H, as well as leads to a reduction of the XH σ* acceptor orbital energy.

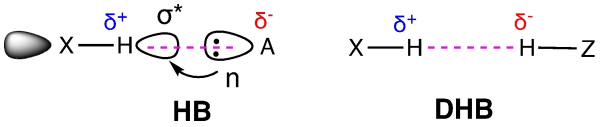

Scheme 1. Comparing hydrogen bonding (**HB**) to dihydrogen bonding (**DHB**).

More recently, attention has been given to dihydrogen bonding (**DHB**), in which attractions between oppositely polarized hydrogen atoms X–H···H–Z are important (Scheme 1, right).[5–8] The Z atom in **DHB** is generally a metal or electropositive element, so that polarization of the Z–H results in hydridic character onto the hydrogen atom, which can then better interact with the acidic or positively charged hydrogen atom of X–Y. Less prevalent than **HB** interactions, **DHB** interactions can be weaker and more subtle than conventional **HB** interactions. As one might expect, as the difference in electronegativity of Z and H, and/or X and H, grows smaller, the strength of both **HB** and **DHB** interactions would be reduced due to decreased electrostatic interactions. **HB** involving non-polar phosphorus-hydrogen bonds, for example, are less common than those involving nitrogen-hydrogen bonds.

Interest in **DHB** involving phosphorus centers has grown tremendously with the reports of reversible activation of dihydrogen by Frustrated Lewis Pairs (FLP) systems.[9] The heterolytic splitting of dihydrogen across select P and B centers

[a] *A. M. Stone, A. R. Golden, S. M. Daniel, J. D. Protasiewicz*
Department of Chemistry, Case Western Reserve University, 2080 Adelbert Road, Cleveland, Ohio 44106, United States
E-mail: protasiewicz@case.edu

[b] *A. L. Rheingold*
Department of Chemistry and Biochemistry, University of California, San Diego, La Jolla, California 92093, United States

Supporting information for this article is available on the WWW under https://doi.org/10.1002/ejic.202400260

Research Article
doi.org/10.1002/ejic.202400260

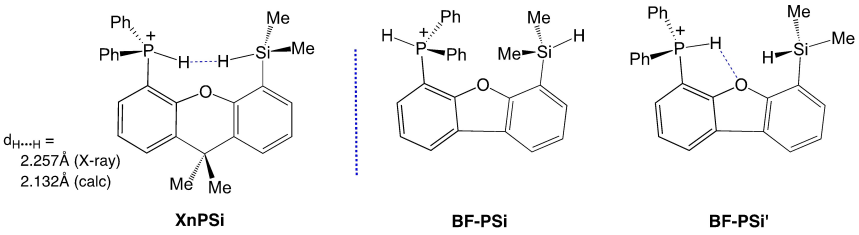

Scheme 2. Example of previously examined PH···HSi **DHB** systems.

can produce close H···H contacts suggesting the presence of bridging **DHB** across some newly generated phosphonium and borohydride centers.[10] Thus, **DHB** may be implicated as playing a role during reversible activation of dihydrogen by main group compounds.[11] While most studies of **DHB** involving PH bonds involve polar BH bonds of various FLP systems, evidence for cases of **DHB** involving PH bonds with relatively non-polar EH bonds is much more limited. For example, protonation of 4-diphenylphosphino-5-dimethylsilyl-9,9-dimethylxanthene leads to cationic species **XnPSi** (Scheme 2, left), which shows short PH···HSi contacts.[12] Computational studies are consistent with the presence of attractive **DHB** interactions for these neighboring hydrogen atoms. Upon calculation of isodesmic reactions, the PH···H–Si interaction energy was estimated to be small (ca −0.05 kcal/mol).

Protonation of 4-diphenylphosphino-6-dimethylsilyldibenzofuran to generate the closely related cationic species **BF-PSi**, however, did not lead to DHB interactions. These results show that weak interactions involving two sets of non-polar EH bonds can be realized if geometries of the EH units are predisposed appropriately. In the case of the **BF-PSi** cation, computations also predicted that PH···O interactions (**BF-PSi'**) would be favored over **DHB**.

Part of the challenge of studying **HB** and **DHB** involving neutral organophosphorus compounds lies in the typically air-sensitive nature of organophosphorus compounds, especially those having one or two P–H bonds. In particular, many primary phosphines (RPH_2) are not only unstable in air, but pyrophoric. Also, the presence of sterically encumbered groups on phosphorus often introduced to render kinetic stability to P–H functionalities can hinder studies of $P\text{-}H_n\cdots A$ and $PH_n\cdots H\text{–}Z$ interactions.

ortho-Hydroxyarylphosphines have a very rich chemistry that has been exploited in numerous applications including as building blocks for heterocyclic compounds, ligands for catalysis, dental materials, and functional materials.[13] *ortho*-Phosphinophenol (**oPP**) can be considered the parent compound of this important class of materials. It was first prepared over 40 years ago,[14,15] and is an unusual example of an air-stable primary phosphine.[16,17] Our group has found great utility of this small molecule and its analogues for synthesis of a large variety of luminescent materials featuring low coordinate phosphorus centers.[18]

oPP has been examined by computational methods previously. The earliest report provided an estimate of the rotational barrier about the PC bond (2.6 kcal/mol) at the HF/3–21G(d) level of theory.[19] This study identified the lowest energy conformational isomer as having the OH group directed towards the P atom and the P lone pair directed away from the OH group (**PP4**, Scheme 3).

A subsequent DFT study on over sixty 2-substituted phenols examined intramolecular hydrogen bonding using B3LYP/6-31G(d,p) methodology.[20] Included in this study was **oPP**. Three conformational isomers of **oPP** were identified (**PP1**–**PP3**, Scheme 3). **PP1** was determined to be lower in energy than the other two isomers ($\Delta G = -0.9$–1.0 kcal/mol). An estimate for $\Delta H_{intra\text{-}HB}$ of 0.8 kcal/mol was made based on differences in energies between **PP1** and **PP3** having the OH unit directed either towards or away from the P atom. No mention of an isomer of the form **PP4** was made in this particular study, however.

We became interested in the fine details of **oPP** while examining its oxidation to the oxide **oPP-oxo**, and the subsequent disproportionation of **oPP-oxo** to yield **oPP** and ArP(=O)(OH)H (**oPP-oxo-hydroxy**, Equation (1)).[21] During our theoretical calculations on the starting material **oPP**, we revisited the four potential conformational isomers **PP1**–**PP4**.

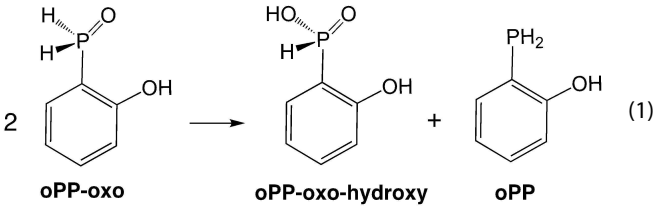

During our study, a systematic DFT analysis of potential conformers for **oPP** (ωB97X-D/6-31G*) confirmed that **PP1**–**PP4** indeed represent minima, and that structure **PP4** lies very close in energy to **PP1** (*vide infra*). This unusual low energy structure piqued our interest, as one might have anticipated **PP4** as being higher in energy than the isomer having favorable geometry for intramolecular **HB** (**PP1**). If **DHB** is active between

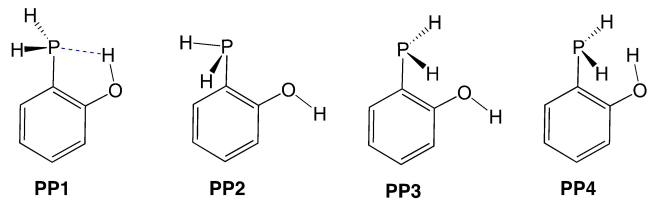

Scheme 3. Four conformations of **oPP**.

Research Article
doi.org/10.1002/ejic.202400260

PH_2 and OH groups, however, this result might imply that for **oPP** the strength of PH···HO dihydrogen bonding rivals or bests the energy for conventional P···HO hydrogen bonding in **PP1**.

An alternative proposal that has received study involves P···HO hydrogen bonding acting in a different and unconventional manner. In these studies, two types of dimers of H_3P and H_2O were determined to be stable *in silico*. One dimer is associated by a conventional intermolecular P···HO hydrogen bond (*syn*), and another is associated with an intermolecular P···HO hydrogen bond whereby the hydrogen bond acceptor (σ*(OH)) avails itself to the electron density located in the backside of the lobe formally containing the phosphorus lone pair (*anti*, Scheme 4). The two studies came to different conclusions.

The first study found a P···H distance of 2.9075 Å and a OH···P bond angle of 169.8° (HF/6-311++G(3df,3pd) and MP2/6-311++G(3df,3pd) methods).[22] After consideration of weak interaction energies, IR data, NBO and AIM analyses, it was concluded that the attraction that holds the *anti* dimer together is not attributable to hydrogen bonding but is mostly stabilized by dispersion energy. A second study revisited this unusual interaction at the MP/aug-cc-pVTZ level of theory.[23] This work also identified an *anti* form of the water-phosphine adduct, having a P···H distance of 2.919 Å and a OH···P bond angle of 165.1°. Both studies found $E_{binding}$ energies of ~1 kcal/mol, but the later study concluded, after probing the association by further suite of theoretical analyses, that a hydrogen bond exists. This study also ponders the existence of finding experimental evidence for this phenomenon, acknowledging the challenges that (a) molecules larger than H_2O and PH_3 will face steric forces arising when groups larger than H are present and (b) electronegative substituents having lone pairs will complicate this weak interaction. Interestingly, **oPP** offers a unique opportunity to examine this possibility for it is relatively unhindered at the phosphorus center and the hydrogen bond acceptor is located in close proximity to phosphorus.

Herein we present experimental evidence for intramolecular and intermolecular **HB** for the air stable primary phosphine *ortho*-phosphinophenol (**oPP**). Furthermore, we present computational evidence for previously unrecognized **DHB** in **oPP**, and that the intramolecular P–H···H–O **DHB** can compete with intramolecular P···H–O HB in **oPP** in the gas phase or non-polar solvents.

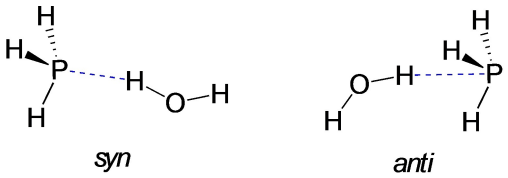

Scheme 4. Conventional (*syn*) and unconventional (*anti*) **HB** between water and PH_3.

Results & Discussion

A search of potential conformers of **oPP** (ωB97X-D/6-31G*) by systematic rotation about CP and CO bonds located the four conformational isomers **PP1**–**PP4** (see SI). At this level of theory isomer **PP1** was lower in energy that **PP4** by only 0.08 kcal/mol. These initial four structures were then further minimized at the ωB97M-V/DEF2-QZVPPD level of theory. The ωB97M-V density functional is a combinatorially optimized range-separated hybrid meta-GCA which has been shown to give high-quality results for main group compounds, especially when large basis sets are used.[24] Interestingly, the ordering of stabilities agrees with the results using the HF/3-21G(d) level of theory, showing that structure **PP4** is indeed predicted to be the lowest energy isomer (Table 1).

This relative ranking was also confirmed by a variety of other higher quality methods and basis sets (including B3LYP-D3 and MP2), all of which consistently placed isomer **PP4** as the lowest energy species (see SI) in the gas phase. Several methods were explored that included corrections for solvent effects. These did not change the fact that *in silico* **PP4** was consistently predicted to be favored by ca 0.3–1.3 kcal/mol over the next lowest energy isomer **PP1** having intramolecular hydrogen bonding. Interestingly, at the MP2/aug-cc-pVQZ level [IEFPCM Cyclohexane] of theory the energy ordering remains as seen for the gas phase (**PP4** < **PP1** < **PP3** < **PP2**), using IEFPCM solvent corrections (Integral Equation Formalism Polarizable Continuum

Table 1. Calculated thermodynamic values for four **oPP** conformations (ωB97M-V/DEF2-QZVPPD//ωB97M-V/DEF2-QZVPPD).

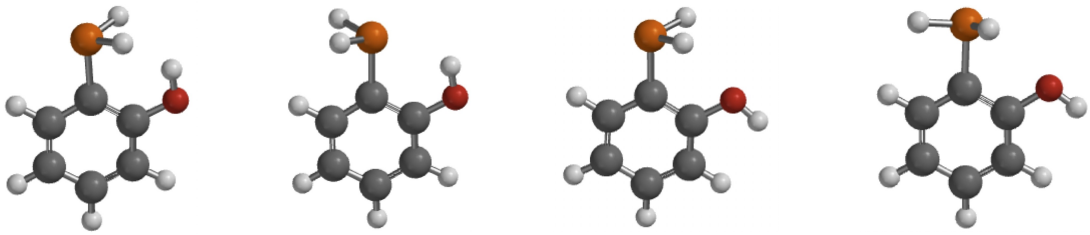

	PP4	PP1	PP3	PP2
Δ E_{elec} (kcal/mol)	0.00	0.98	1.57	1.89
Δ G (kcal/mol)	0.00	0.91	1.30	1.57
Δ H (kcal/mol)	0.00	0.94	1.46	1.76

Research Article
doi.org/10.1002/ejic.202400260

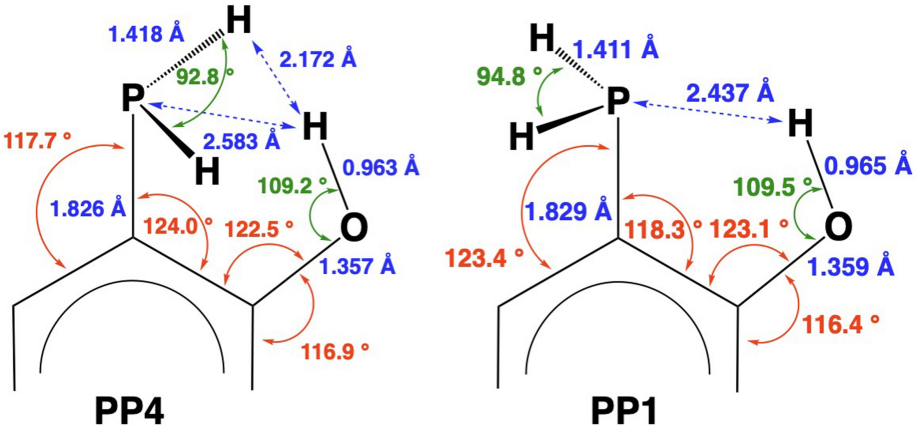

Scheme 5. Comparison of selected computed structural parameters for **PP4** vs **PP1** (ωB97M-V/DEF2-QZVPPD//ωB97M-V/DEF2-QZVPPD).

Model) for either dichloromethane or acetonitrile the ordering changes to **PP4** < **PP2** < **PP3** < **PP1**. Reordering of the isomer energies may thus lead to solvent dependent IR and/or NMR spectra (*vide infra*).

Selected computed structural details for **PP4** and **PP1** (ωB97M-V/DEF2-QZVPPD) are shown in Scheme 5. Both feature short OH···P contacts (2.583 and 2.437 Å, respectively) that are below the sum of the van der Waal radii (2.94 Å). **PP1** also displays a PCC bond angle of less than 120° (118.3°), both attributes being consistent with attractive and conventional **HB** interaction between lone pair on the P atom and the hydroxyl unit. While isomer **PP4** also has a similarly shortened OH···P contact, the feature is accompanied by an increased PCC bond angle which is greater than 120° (124.0°) suggesting OH···P repulsion. Such a repulsive interaction is not consistent with the presence of an unconventional (*anti*) hydrogen bonding interaction. Interestingly, the proximal H···H contacts in **PP4** of 2.17 Å are slightly less than the sum of the van der Waal radii (2.20 Å) and could indicate favorable attractions and **DHB**. If attractive PH···HO **DHB** interactions were present, they might be limited by P···HO repulsive interactions (*vide infra*).

In order to determine the experimental structure of **oPP**, crystals of **oPP** were grown by vapor diffusion of pentane into a concentrated solution of **oPP** in CH_2Cl_2 (DCM), and the results of single crystal X-ray diffraction are shown in Figure 1. Hydrogen atoms on the O and P atoms were successfully located in the difference maps and their positions refined (other H atoms at idealized positions).

Metrics within the molecule are not unusual, and the overall structure is quite similar to that computed for isomer **PP2**. Scheme 6 shows a side by side comparison of the metrics for experimental structure and the calculated structure (ωB97M-V/DEF2-QZVPPD). The main exception noted is that the experimentally determined PH and OH distances are shorter due to the nature of single crystal X-ray diffraction studies which rely on diffraction from electrons.

The molecules of **oPP** in the crystalline solid state associate via intermolecular hydrogen bonds from neighboring P and OH functionalities. This type of aggregation was previously reported for (Ar)(Ph)^{t}BuP (Ar = 4-Me-2-OH-C_6H_3),[25] which showed

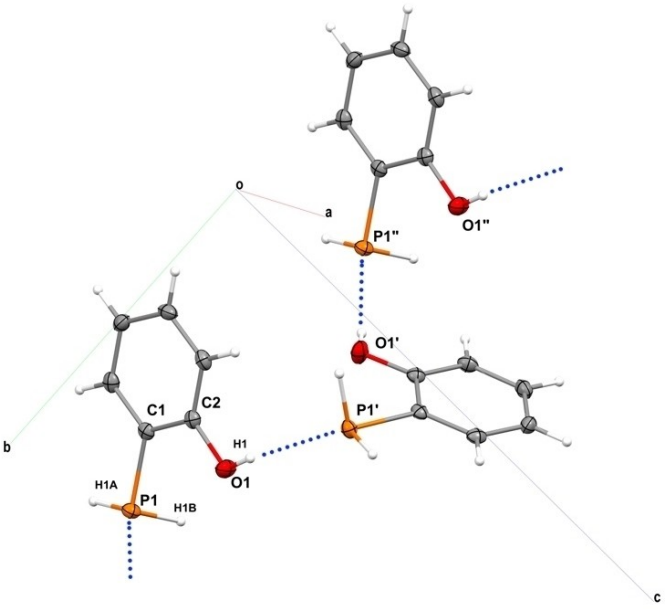

Figure 1. Structure of **oPP** in solid state highlighting intermolecular P···HO hydrogen bonds linking individual molecules in the unit cell. For selected bond distance and angles see Scheme 6 (left).

a P···H distance of 2.42 Å and an OH···P angle of 152° (166.0° for **PP2**). By contrast, the structure of related (Ar)(Ph)^{t}BuP (Ar = 3,5-^{t}Bu$_2$-2-OH-C_6H_3) finds the hydroxyl group oriented toward the P atom suggesting intramolecular hydrogen bonding (P···H distance of 2.48 Å and OH···P angle of 123.6°).

Hydrogen bonds can often be inferred by bond critical points during examination by the Atoms in Molecule theory,[26] and also be visualized by regions of attractions produced by non-covalent interaction (NCI) plots.[27] One pair of molecules from the X-ray structure of **oPP** were analyzed at the B3LYP-D3/6-311++G(2d,2p) level of theory (after adjusting PH and OH bond lengths for artificial contractions produced by X-ray method). The NCI plot (Figure 2, left) shows a blue-green disc indicative of a strong attraction between the hydroxyl-H and P atoms. A bond critical point (Figure 2, right) between the H and P atoms reinforces the proposal of a significant **HB** between

Research Article
doi.org/10.1002/ejic.202400260

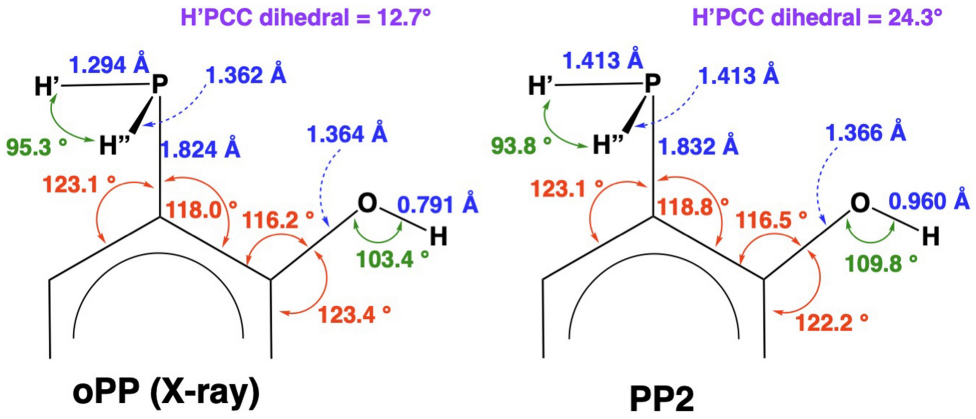

Scheme 6. Comparison of selected X-ray crystallographically determined structural parameters of **oPP** vs corresponding computed parameters for **PP2** (ωB97M-V/DEF2-QZVPPD//ωB97M-V/DEF2-QZVPPD).

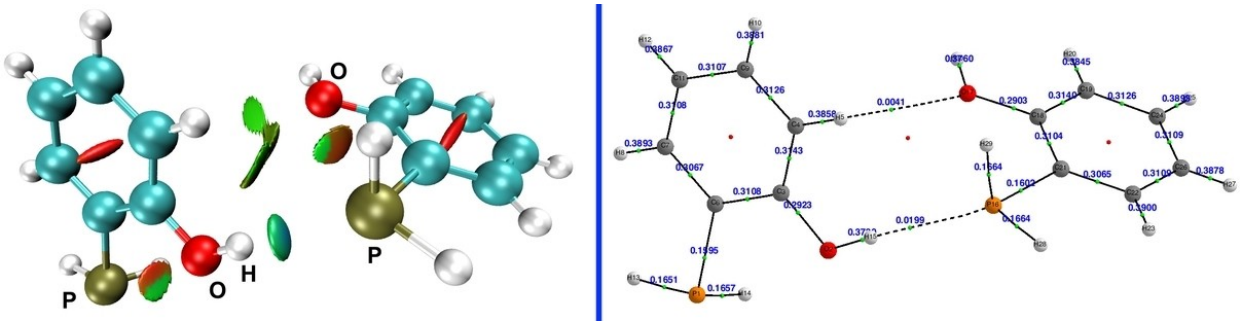

Figure 2. NCI plot (left) for **oPP** in solid state crystal structure. The surface color red indicates repulsions, green van der Waals attractions and/or weak interactions, and blue stronger attractive interactions. BCPs (right) from AIM analysis for **oPP** in solid state crystal structure.

these atoms. The analysis also suggests weak intermolecular interactions in the solid state between the O atoms and neighboring CH groups. The favorability of **oPP** adopting the form of **PP2** for packing in the solid state is probably driven by the ability to adopt of near linear OH···P geometries which are unobtainable by intramolecular **HB**.

Having rigorously established the presence of OH···P **HB** for **oPP** in the solid state, it was of interest to investigate the reasons for conformational isomer **PP4** having the lowest energy, and to collect evidence (computational and experimental) for previously unrecognized bifurcated PH···HO **DHB** as a stabilizing force in **oPP**. Also of interest is an unusual opportunity to compare and contrast **HB** and **DHB** within the same molecule and functional groups.

Applying similar analyses as employed above, the four lowest lying conformational isomers of **oPP** were examined using MP2/aug-cc-pVTZ//ωB97M-V/DEF2-QZVPPD level of calculations, and the wavefunctions analyzed by Multiwfn and AIMAll.[28] The resulting contour line maps of the Laplacian of electron density with bond paths and bond critical points of electron density for **PP1** and **PP4** are shown in Figure 3 (corresponding figures for **PP2** and **PP3** available in SI).

A bond critical point is found along the OH···P **HB** path for **PP1**, with a rho value of 0.0195 au, while none were located that would correlate for OH···HP **DHB** in **PP4**. The lack of an OH···HP bond critical point in and of itself can not be taken to indicate the absence of hydrogen bonding.[29] For example, it has recently been shown that certain 1,n-alkanediols can lack bond critical points yet show evidence for hydrogen bonding in electron density plots.[30]

The corresponding non-covalent interaction (NCI) plots (Figure 4a and b, insets), however, reveal both similarities and differences (Figure 4a and b). Both feature regions of attractive and repulsive interactions between the H and P atoms (surface color red indicates repulsion, green weak attractions). An attractive surface for **PP1** is located directly between the H and P atoms. The green color indicates the attraction is weaker than that observed for intermolecular **HB** in crystals of **oPP** which are indicated in blue.

The attractive NCI surface regions for **PP4**, however, are concentrated between the three hydrogen atoms, consistent with the presence of dihydrogen bonding. Looking at the details for the computed structures of **PP1** and **PP4** (Scheme 5), one notes that the CCP bond angle is 7.7° larger (124°) in **PP4** than **PP1**, consistent with OH···P repulsive interactions. The HPH bond angle in **PP4** is 2° smaller than that in **PP1**, which might be taken as a distortion induced as the chelating phosphorus-hydrogens' embrace the hydrogen on the hydroxyl group. These data also argue that the unconventional hydrogen

Research Article
doi.org/10.1002/ejic.202400260

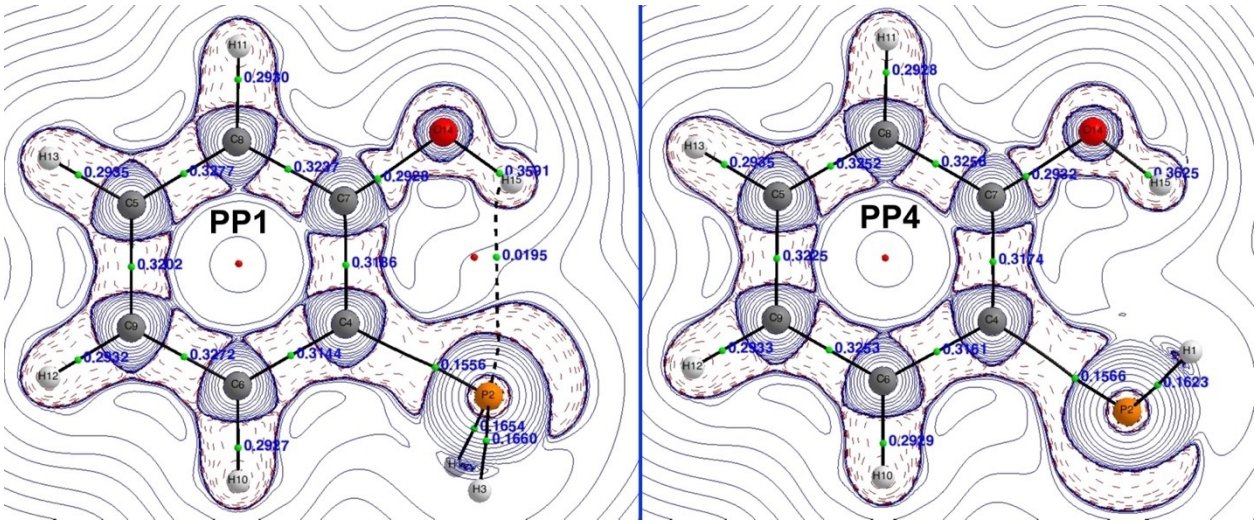

Figure 3. Contour line maps of Laplacian of electron density with bond paths, and CPs (green spheres) and RCPs (red spheres) in au for **PP1** (left) and **PP4** (right).

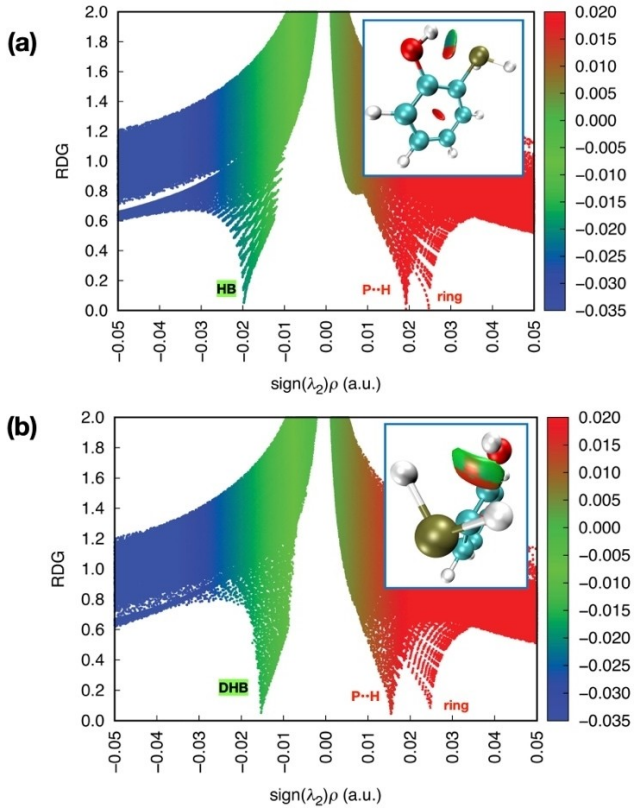

Figure 4. Reduced density gradient (RDG) plots for **PP1** (a) and **PP4** (b) with corresponding insets for the NCI plots. The surface color red indicates repulsions, green van der Waals attractions and/or weak interactions, and blue stronger attractive interactions.

bonding (*anti*) suggested between water and phosphine dimers does not play a role here.

The reduced density gradient (RDG) data (Figure 4) for these two conformational isomers highlights the interesting fact that the **HB** interaction in **PP1** is stronger (ca 0.020 au electron density) compared to the **DHB** interaction in **PP4** (ca 0.015 au electron density). Isomer **PP4**, however, contains two such attractive interactions, thus contributing to the order of overall stability. Similarly the repulsive P···H interactions found in **PP4** are smaller than in **PP1**, although, again, one must be considered for each bound hydrogen.

Another means to probe these interactions in **PP1** and **PP4** is by Natural Bond Orbital (NBO) methods.[31] This approach allows one to visualize localized orbitals and to explore interactions between pairs of NBOs. Overlapping relevant NBOs for **PP4** and **PP1** are shown in Figure 5. The lone pair on phosphorus is shown either directed away from or towards the hydrogen atom and associated σ*(OH) orbital for each isomer. The key output of the second order perturbation theory analysis of the Fock matrix in NBO for the two isomers reveals, perhaps not unexpectedly, a much weaker interaction (6.6 times) for **PP4** relative to **PP1**. If one accepts that conventional hydrogen bonding exists in **PP1**, and that it is worth ca 1 kcal/mol, then it stands to reason that at least the donor-acceptor part of hydrogen bonding of **PP4** is worth at most 0.15 kcal/mol (15 %) of that in **PP1**. This much greater lack of spatial overlap may contribute to the lack of a bond critical point in the AIM analysis for **PP4**. Donor-acceptor interactions between PH and OH bonds in **PP4** were not identified by this analysis, indicating that these potential interactions are probably below the threshold for printing.

Furthermore, examination of the NBO atomic charges suggests that the P–H hydrogens are negatively polarized, which can thus collectively contribute to electrostatic attractions between the two P–H hydrogens and acidic (positively charged) hydroxyl proton (P: 0.466, PH: −0.081, OH: 0.483, see also Figure S54 in SI). The presence of dihydrogen bonding between non-polar main group hydrides and alcohols is not without precedent. For example, trialkylsilanes (R_3SiH) have been shown to interact with various acidic alcohols.[32] In cyclohexane, the association of perfluoro-*tert*-butanol ($(CF_3)_3COH$) with trihexylsilane by Si–H···H–O interactions was

Research Article
doi.org/10.1002/ejic.202400260

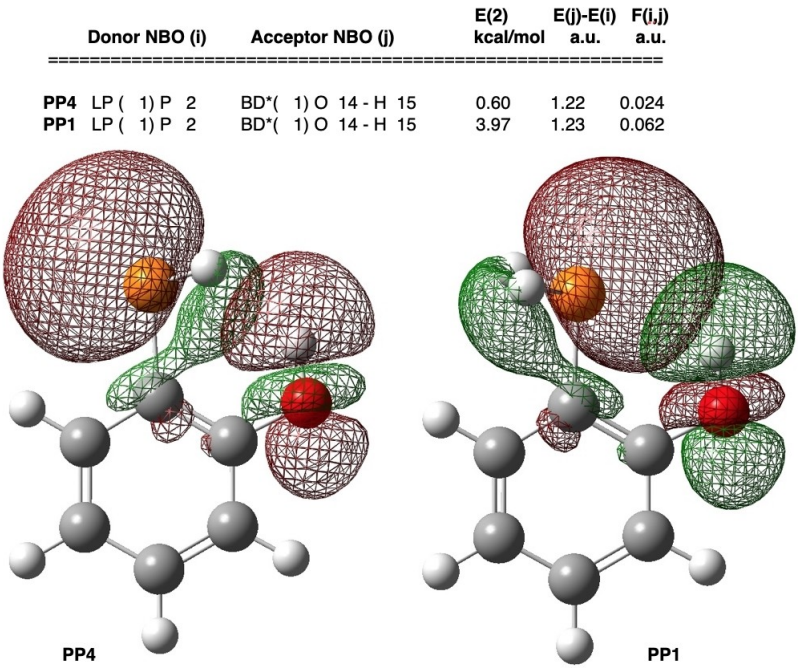

Figure 5. NBO analysis of conformational isomer **PP4** vs **PP1** (MP2/aug-cc-pVTZ//ωB97M-V/DEF2-QZVPPD).

measured as 0.8 M^{-1} and computed to be equally small in the gas phase. As noted in this work, gas phase calculations do not appropriately account for dampening effects of competitive dispersion with solvent. Combined spectroscopic (laser-induced fluorescence and IR) and theoretical (DFT) study of the interactions of diethylmethylsilane (Et_2MeSiH) and triethylsilane (TES, Et_3SiH) with phenol revealed the presence of multiple types of possible isomers.[33] For TES-phenol dimers, four adducts were observed with red shifted ν_{OH} bands (31–78 cm^{-1}) by IR-UV double resonance spectroscopy. Structures analyzed by DFT methods (M05-2X/6-311++G(3d,2p)) showed red shifted ν_{OH} bands (5–82 cm^{-1}).

As a means to provide further assessment of energetics for **DHB** and **HB** in **PP1** and **PP4**, a pair of isodesmic calculations (MP2/aug-cc-pVTZ//MP2/aug-cc-pVTZ) were carried out on the reactions in Scheme 7(left). The results show values of −2.57 kcal/mol for bifurcated **DHB** in **PP4** and −1.7 kcal/mol for **HB** in **PP1**. Interestingly, upon exchange of one H atom in **oPP** for a methyl group (**HMePP**, Scheme 7right), the order is reversed and **HB** is favored over **DHB** (−2.38 vs −1.73 kcal/mol). An example of a structure having potential bifurcated PH_2···HN **DHB** has been reported, but the H···H contacts are longer at 2.27 and 2.35 Å as determined by single crystal X-ray diffraction studies.[34] Bifurcated SiOH···H_2B **DHB** has also been recently reported.[35] Computational studies on a different type of intramolecular bifurcated DHB having two rings have also been reported.[36]

Since these attractive interactions are weak, it is clear that other factors will play an important role in dictating which structure is realized in the wild (i.e., *ex silico*). As already presented, in the solid state **oPP** adopts the form of **PP2** which can maximize stronger intermolecular **HB** assembly. In solution, it is highly probable that solvation effects will play a strong role. It was thus of interest to examine NMR and IR spectroscopic

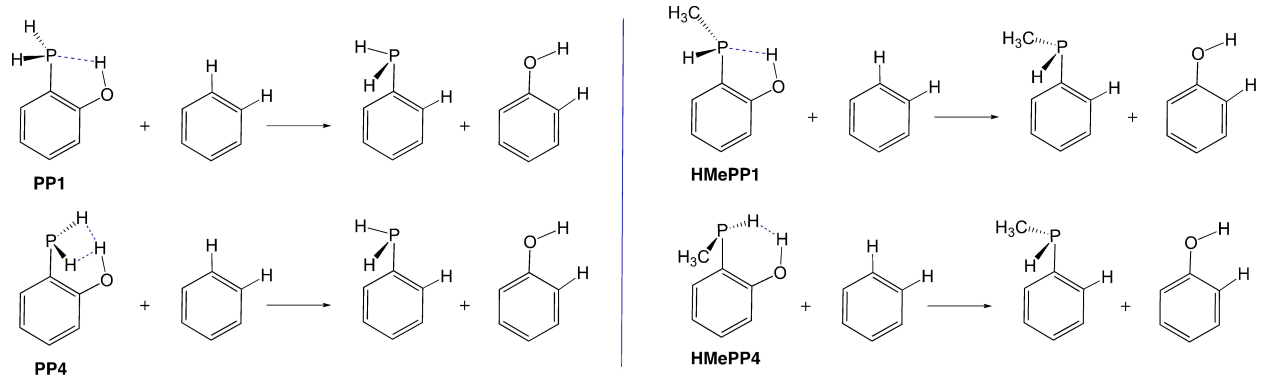

Scheme 7. Isodesmic reactions used to assess energies of **HB** and **DHB** for **oPP** and **HMePP**.

Research Article
doi.org/10.1002/ejic.202400260

properties for **oPP** in various solvents. Given that the energy differences between the four conformational isomers is small (< 2 kcal/mol), and that energy profile scans (ωB397X-D/6-31G*, see SI) of rotations about the PC and OC bonds suggest barriers less than 4 kcal/mol, interconversions of the four potential isomers might be expected to be rapid on the NMR timescale, and possibly be solvent dependent.

^{31}P NMR spectroscopic studies of **oPP** in various solvents (Table 2) reveal a significant solvent dependency (ca 17 ppm) for the ^{31}P NMR chemical shifts. In general, chemical shifts move upfield as the solvent becomes less polar. No significant changes in the PH coupling constant are induced however. While the shifts in general track with solvent polarity, plots of data against standard types of solvent parameters (such as dielectric constant, dipole moment, refractive index, and normalized transition energies) were not linear (see SI). The ^{1}H NMR chemical shifts of the PH_2 protons varied slightly between 3.54 and 4.02 ppm, and in a fashion not also readily correlated with solvent polarity. The ^{1}H NMR signals for the hydroxyl proton shifted greatly, presumably in response to varying types and degrees of hydrogen bond interactions.

The significance of hydrogen bonding on ^{31}P NMR shifts is easily demonstrated by noting the impact of HB acceptors to solutions of **oPP**. In $CDCl_3$, addition of 1.5 equivalents of NEt_3 to **oPP** induces a shift of the ^{31}P NMR resonance from δ −154.2 to −140.6 ppm with virtually no change in J_{PH} (204–205 Hz). Likewise, addition of 1.5 equivalents of pyridine to **oPP** In $CDCl_3$, induces a shift of the ^{31}P NMR resonance from δ −154.2 to −141.5 ppm, again with virtually no change in J_{PH} (203–205 Hz). Interestingly, this chemical shift is near that found for **oPP** in neat pyridine-d_5 (δ −140.2 ppm). The impact of **HB** on the ^{1}H NMR resonances for the PH_2 protons is less pronounced, with δ 3.77 vs δ 3.70 (w/1.5 NEt_3 added) and δ 3.84 (w/1.5 pyridine added). The OH protons, however, shift dramatically with δ 4.97 for pure **oPP** in $CDCl_3$, vs δ 11.35 (w/1.5 NEt_3 added) and δ 10.59 (very broad, w/1.5 pyridine added). By contrast, even when **oPP** is dissolved in acetic acid, no evidence for protonation of phosphorus is noted.

A method to quantify the hydrogen bonding acceptor capabilities of solvents has been developed based on the ^{19}F NMR chemical shifts of *para*-fluorophenol relative to *para*-fluoroanisol.[38] Using solvatomagnetic β_1 values that are available for specific solvents in Table 2, one can correlate the ^{31}P chemical shifts for *ortho*-phosphinophenol with β_1 values, as shown in Figure 6. Interestingly, the ^{31}P NMR shift for **oPP** in acetic acid follows the trend for other solvents, thus indicating this solvent acts primarily as a **HB** acceptor despite the potentially basic phosphorus center. Overall, these results show that direct solvent interactions are much more significant on the ^{31}P NMR shifts than those induced by simple computed field effects.

Despite the fortuitous structural similarities between *para*-fluorophenol and *ortho*-phosphinophenol, the relationship is not perfect. Discrepancies from linearity are likely attributable

Table 2. ^{31}P and ^{1}H NMR data for **oPP** in different solvents (and selected solvent parameters).

Solvent	Dielectric Constant (ε)	Solvatomagnetic β_1	PH_2 ^{31}P NMR δ (ppm), J_{HP} (Hz)	PH_2 ^{1}H NMR δ (ppm)	OH ^{1}H NMR δ
D_2O	80.1	0.37	−144.5, 211	3.75	4.75
Dimethylsulfoxide-d_6	46.7	0.71	−139.3, 204	3.71	9.93
Acetonitrile-d_3	37.5	0.37	−144.6, 203	3.78	7.31
Dimethylformamide-d_7	36.7	0.69	−142.3, 201	3.77	10.21
Methanol-d_4	32.7	0.54	−146.1, 202	3.73	4.91
Acetone-d_6[a]	20.7	0.49	−144.6, 202	3.77	8.77
Pyridine-d_5	12.4	0.69	−140.2, 202	4.10	12.17
Dichloromethane	8.93	–	−152.4, 204	–	–
Acetic acid	6.17	0.38	−145.8, 200	–	–
Chloroform-d	4.81	–	−154.2, 205	3.77	4.97
Chloroform-d + 1.5 eq NEt_3	–	–	*−140.6, 204*	*3.70*	*11.35*
Chloroform-d + 1.5 eq py	–	–	*−141.5, 203*	*3.84*	*10.59*
Chloroform-d + 1.5 eq MeCN	–	–	*−149.2, 204*	*3.78*	*6.06*
Diethyl Ether	4.33	0.59	−146.1, 198	–	–
Carbon Disulfide	2.64	–	−153.7, 201	4.02	5.51
Toluene	2.38	0.15	−152.9, 202	–	–
Benzene-d_6	2.27	0.14	−153.6, 203	3.54	4.41
Carbon Tetrachloride	2.24	–	−156.0, 206	3.89	5.38
Cyclohexane-d_{12}	2.02	0	−160.0, 202	3.61	5.28
Pentane	1.84	0	−161.7, 199	–	–

[a] Reaction occurs.[37]

Research Article
doi.org/10.1002/ejic.202400260

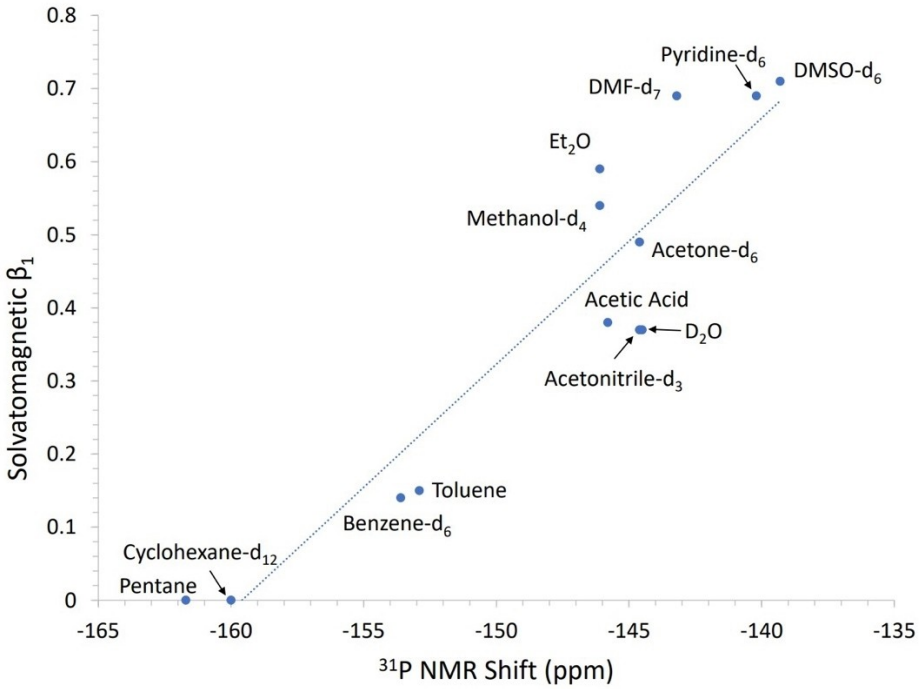

Figure 6. Plot of solvatomagentic β_1 values versus ^{31}P NMR chemical shifts of **oPP** in various solvents.

to a combination of secondary factors. These include the fact that the ^{31}P NMR "reporter" PH_2 group in **oPP** is located on a non-innocent *ortho*-position in the phenol, thus allowing for the possibility of competitive intramolecular **HB**/**DHB** interactions. One or more of the following phenomena could also influence ^{31}P NMR chemical shifts: (a) intramolecular proton transfer from O to P to produce equilibrium amounts of a zwitterion salt, (b) a changing distribution of **oPP** isomers (**PP1**–**PP4** above) with solvent polarity, (c) self aggregation of the **PP1**–**PP4** into dimers $(\mathbf{oPP})_2$ or aggregates of higher order, and (d) unique solvent (**S**) associated species **oPP•S** formed by combination of hydrogen bonding and/or π-interactions that not only include OH but also PH_2 functionalities. Possibilities a–d are assessed by combined computational and IR spectroscopic studies below.

DFT calculations (ωB97M-V/DEF2-QZVPPD//ωB97M-V/DEF2-QZVPPD) on the zwitterionic form of **oPP** (**PPZ**) were undertaken. The key differences between the computed structures of **PP4** and **PPZ** are compared in Scheme 8. The zwitterionic form displays severe distortions to bring the sites of opposite charge towards one another, creating about a 30° difference between the two CCP bond angles. The predicted energy differences between **oPP** isomers **PP4** and **PPZ** is 26.6 kcal/mol in the gas phase. Likewise, using the B3LYP-D3(BJ)/6-311++G(d,p) methodology gave a comparable geometry for **PPZ** (see SI Figure S66) and energy difference (28.4 kcal/mol). Since the charge localization may be stabilized by polar solvents, calculations with solvent corrections B3LYP-D3(BJ)/6-311++G(d,p) [IEFPCM Solv]//B3LYP-D3(BJ)/6-311++G(d,p) [IEFPCM Solv] (S= dichloromethane or DMSO) were undertaken. The energy differences for dichloromethane and DMSO dropped to 20.7 and

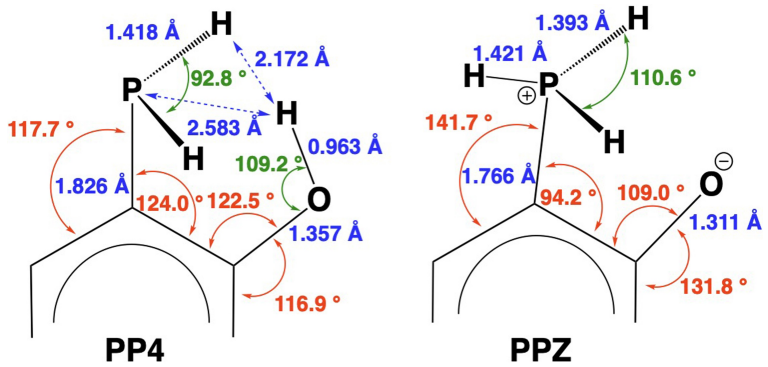

Scheme 8. Comparison of selected computed structural parameters for **PP4** vs **PPZ** (ωB97M-V/DEF2-QZVPPD//ωB97M-V/DEF2-QZVPPD).

Research Article
doi.org/10.1002/ejic.202400260

Table 3. Computed ^{31}P NMR shifts for **oPP** conformational isomers.

	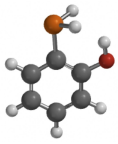 PP4	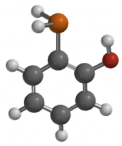 PP1	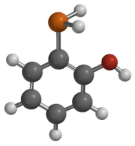 PP3	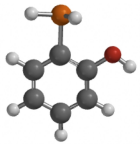 PP2
DFT Methods & Basis Sets	δ	δ	δ	δ
PBE1PBE/6-311G++(2d,2p)// PBE1PBE/6-311G++(2d,2p)	*−209.3*	*−178.1*	*−193.1*	*−150.4*
PBE1PBE/6-311G++(2d,2p) [IEFPCM CH_2Cl_2]// PBE1PBE/6-311G++(2d,2p) [IEFPCM CH_2Cl_2]	*−207.2*	*−178.4*	*−191.9*	*−150.0*
PBE1PBE/6-311G++(2d,2p) [IEFPCM Water]// PBE1PBE/6-311G++(2d,2p) [IEFPCM Water]	*−206.6*	*−178.4*	*−191.5*	*−150.0*

19.1 kcal/mol, respectively. These energies alone would suggest insufficient **PPZ** is present that could influence the ^{31}P NMR chemical shifts. While specific hydrogen bonding is not included in these calculations, the lack of significant impact of $J(PH_2)$ values across the broad range of solvents supports the proposition that the phosphorus center in **oPP** in solution remains largely unprotonated.

Averaged ^{31}P NMR chemical shifts could also conceivably vary across different solvents if the distribution of conformational isomers **PP1**–**PP4** occurs with changing solvents, and if the isomers have significant ^{31}P NMR chemical shift differences (*vide supra*). Calculations of the ^{31}P NMR chemical shifts of isomers **PP1**–**PP4** were thus undertaken to examine predicted differences in chemical shifts between the isomers. The PBE1PBE/6-311G DFT method, that has been shown to give good results across a range for organophosphorus compounds, was employed.[39,40] The results show (Table 3) that the shifts are remarkably dependent on the specific orientations of PH_2 and OH functional groups with respect to one another ($\Delta\ \delta >$ 50 ppm). Interestingly, the calculated chemical shift of −150 ppm for isomer **PP2** (the X-ray determined isomer), falls within the range of the shifts experimentally determined and could be considered a reasonable match. The three other isomers are predicted to display shifts notably further upfield. Examination of some other methods for calculating ^{31}P chemical shifts gave comparable results (see SI). Calculations of ^{31}P NMR shifts using solvent corrections (polarizable continuum model IEFPCM) produced only small $\Delta\ \delta < 3$ ppm for individual isomers upon going from gas phase to a very polar solvent such as water. Polarizable continuum models are limited, however, to solute-solvent interactions of electrostatic origin. Combined with calculations that predict only subtle shifts in isomer distribution across several solvents (vide supra), these results add further support the finding that intermolecular hydrogen bonding is a key contributor to solvent effects on ^{31}P NMR shifts.[41] Solvents can also play a large role in disrupting intramolecular hydrogen bonding. Furthermore, self-aggregation for related compounds, such as phenol, is well documented. It also should be mentioned that calculations of ^{31}P NMR shifts are reliable to approximately a mean absolute deviation/root mean square deviation (MAD/RMSD) between 4–10 ppm depending on exact methodology and if (and which) training sets are used.[42]

Hydrogen bonded association of phenol in solution has been studied by combined IR and theory methods.[43] In order to gain deeper insights into the solution phase behavior of **oPP**, infrared (IR) spectroscopic studies of **oPP** in solution were undertaken. Infrared spectroscopy operates on a much faster timescale and offers the opportunity to identify individual isomers in solution. **oPP** features a polar OH bond which can be used as a spectroscopic handle to ascertain hydrogen bonding. IR spectroscopic studies of phenol and substituted phenols have revealed a plethora of ways by which self aggregation and association with solvents might occur.[44]

IR data were thus collected in several representative solvents having suitable transparent windows to allow observation of OH, and in some cases, PH_2 modes. These data, along with solid-state data, are presented in Table 4. In solution, the behavior can be grouped into three groups: dichloromethane, aromatic (benzene and toluene), and non-polar (CS_2, CCl_4, cyclohexane and pentane) solvents. The data from the non-polar solvents (where solvent-solute intermolecular **HB** is

Table 4. Selected solid-state and solution phase IR data for **oPP**.

	OH	PH_2
Solid	3407 (sh), 3308 (s, br), 3217 (sh)	2345 (m), 2297 (s)
Dichloromethane	3684 (w), 3570 (s, br), 3548 (sh), 3501 (sh)	2312 (m), 2293 (m)
Benzene	3543 (s, br)	2300 (m, br), 2279 (sh)
Toluene	3536 (s, br)	2296 (m, br), 2276 (sh)
Carbon Disulfide	3582 (s), 3546 (s), 3498 (m)	–
CCl_4	3606 (s), 3558 (s), 3506 (m)	2303 (s), 2270 (s)
Cyclohexane	3612 (s), 3559 (s), 3512 (m)	2298 (s), 2268 (s)
Pentane	3617 (s), 3563 (s), 3513 (m)	2299 (s), 2271 (s)

Research Article
doi.org/10.1002/ejic.202400260

expected to be minimal) are similar and show multiple OH bands. The similarity of spectra across these solvents is particularly intriguing and could indicate the coexistence of the four isomers **PP1**–**PP4**.

For the non-polar solvents, the IR data could be analyzed and 4 bands could be deconvoluted, not just the 3 that are discerned by eye. Figure 7 shows the results from analysis of **oPP** in cyclohexane (for similar analyses for CS_2, CCl_4, and pentane, see SI). The observed OH modes are higher than what would be expected if strong OH···H or OH···P hydrogen bonding was present (compare to solid **oPP**, Table 4).

Thus it was of interest to determine if experimental data could be assigned using computed IR frequencies for **PP1**–**PP4**. The harmonic OH and PH_2 modes for **PP1**–**PP4** using (a) ωB97M-V/DEF2-QZVPPD//ωB97M-V/DEF2-QZVPPD, (b) MP2 aug-cc-PVTZ [IEFPCM Cyclohexane]//MP2 aug-cc-PVTZ [IEFPCM Cyclohexane], and (c) B3LYP-D3(BJ)/6-311++G(d,p) [IEFPCM Cyclohexane]//B3LYP-D3(BJ)/6-311++G(d,p) [IEFPCM Cyclohexane] methods are shown in Table 5. For the ωB97M-V/DEF2-QZVPPD//ωB97M-V/DEF2-QZVPPD method, optimal scaling factors for this combination of method and basis set do not appear to be available, thus those reported for def2-TZVPPD (0.95) were used.[45]

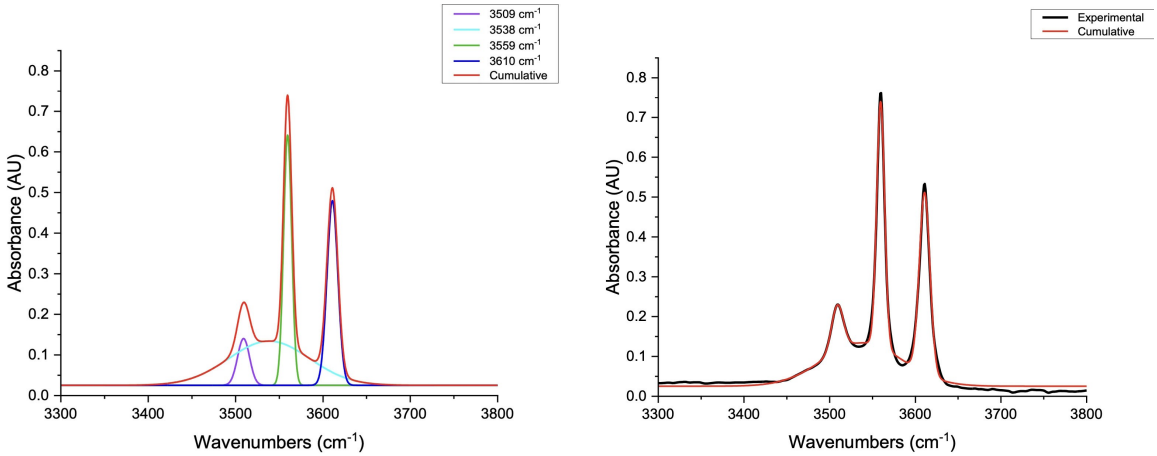

Peak	Wavenumbers (cm^{-1})	Width at Half Height	Integrated Values
Fit Peak 1	3509 (w)	16.13	0.0686
Fit Peak 2	3538 (w, br)	108.85	0.4370
Fit Peak 3	3559 (s)	10.85	0.2469
Fit Peak 4	3610 (s)	14.75	0.2475

Figure 7. Deconvolution and fitting of IR data for **oPP** in cyclohexane.

Table 5. Computed IR data (cm^{-1}) for **PP1**–**PP4**, using (a) ωB97M-V/DEF2-QZVPPD//ωB97M-V/DEF2-QZVPPD, (b) MP2 aug-cc-PVTZ [IEFPCM Cyclohexane]//MP2 aug-cc-PVTZ [IEFPCM Cyclohexane], and (c) B3LYP-D3(BJ)/6-311++G(d,p) [IEFPCM Cyclohexane]//B3LYP-D3(BJ)/6-311++G(d,p) [IEFPCM Cyclohexane].

		ωB97 M-V			MP2		B3LYP-D3(BJ)	
Isomer	Mode #	Freq (Harmonic)	Scaled Freq (Harmonic)	Freq (Harmonic)	Scaled Freq (Harmonic)	Freq (Harmonic)	Scaled Freq (Harmonic)	Freq (Anharmonic)
PP1	33	2440.4	2318.4	2475.4	2376.4	2401.4	2305.3	2313.3
	34	2446.4	2324.1	2483.3	2384.0	2404.6	2308.4	2311.3
	39	3751.4	3563.8	3689.4	3542.2	3701.4	3553.4	3505.2
PP2	33	2421.3	2300.2	2455.6	2357.3	2379.2	2284.0	2281.6
	34	2429.3	2307.8	2469.8	2371.0	2392.6	2296.9	2291.2
	39	3864.9	3671.6	3805.5	3653.3	3830.3	3677.1	3596.1
PP3	33	2416.1	2295.3	2456.1	2358.0	2381.9	2286.0	2286.0
	34	2420.9	2299.9	2460.1	2361.7	2382.4	2286.5	2290.2
	39	3853.4	3660.7	3796.9	3645.8	3821.5	3668.7	3675.3
PP4	33	2381.4	2262.3	2424.9	2327.9	2349.0	2255.0	2213.8
	34	2387.4	2268.0	2428.0	2330.9	2350.8	2256.7	2225.8
	39	3804.7	3614.5	3752.0	3601.9	3773.2	3622.3	3572.7

Research Article
doi.org/10.1002/ejic.202400260

The three methods yield harmonic OH modes for the four isomers that span the ranges of (a) 3564–3672 cm^{-1}, (b) 3542–3653 cm^{-1}, and (c) 3553–3675 cm^{-1}, respectively. Thus all three methods are near the range of experimentally observed OH modes in cyclohexane that span 3509–3610 cm^{-1}. All three methods yielded the lowest frequency OH modes for isomer **PP1** (by 51–69 cm^{-1} to the isomer having the next lowest OH frequency). The lower frequency for **PP1** compared to the other isomers is consistent with the presence of a conventional intramolecular **HB**. The order of frequencies for all three sets of harmonic data is **PP1** < **PP4** < **PP3** < **PP2**.

The observed PH modes in cyclohexane are 2298 and 2268 cm^{-1} (see SI). The three computational methods yield a-c harmonic PH modes for **PP1**–**PP4** that span the ranges of (a) 2262–2324 cm^{-1}, (b) 2328–2384 cm^{-1}, and (c) 2255–2308 cm^{-1}, respectively. **PP1**, by all three methods, exhibits the highest frequency PH modes, resulting from the presence of the **HB** interaction. The frequencies for the PH modes in **PP4**, corresponding to the **DHB** interaction, displays the lowest frequency PH modes across all methods. Unlike with the OH calculations, for which 4 distinct modes could be experimentally discerned, only two could be resolved for the PH modes. If all four isomers are represented in solution, it is likely the smaller dispersions of the PH frequencies will lead to overlapping bands that are not readily resolved.

While the calculated range of harmonic frequencies is in the ballpark of experimental values, we also undertook calculations of anharmonic frequencies to check on the quality of the results since it has been reported that significant errors can occur for even simple PH containing phosphorus molecules such as PH_3.[46] The Generalized Vibrational Second-order Perturbation Theory (GVPT2) approximation[47] within Gaussian 16 was used (anharmonic method allowing calculation of overtones and combination bands with fundamental frequencies) in conjunction with the computationally less expensive B3LYP-D3(BJ)/6-311++G(d,p) method.[48] In general, the anharmonic PH modes for **PP1**–**PP3** are in very good agreement with the corresponding harmonic PH modes (< 10 cm^{-1}). For isomer **PP4**, the differences in PH frequencies are notably larger (31–41 cm^{-1}).

The OH modes determined by anharmonic method show much greater variance compared to those computed using harmonic values (method c). The OH frequencies are lowered by 48–81 cm^{-1} for **PP1**, **PP2**, and **PP4**, while increased slightly for **PP3**, yielding a range of values that span from 3505–3675 cm^{-1} (compare experimental observed in cyclohexane, 3509–3610 cm^{-1}). While none of the sets of harmonic and anharmonic calculated frequencies are an exact match, all three sets cast a reasonable net over the range of observed OH frequencies and support the assignment of the spectra attributable to four isomers of **oPP** coexisting in non-polar solvents, considering the limitations of these computational methods and assumptions. However, we note that one of the observed OH modes is particularly broad relative to the others (3538 cm^{-1}), suggesting that this particular mode is likely attributable to one isomer (**PP1**) having intramolecular **HB**. This assignment, however, is at odds with the expectation that **HB** should produce the lowest frequency (as predicted by calculation). This might signify that one (or more) of the observed bands could be attributed to aggregation of **oPP** in solution (*vide infra*).

The IR spectra of **oPP** in benzene and toluene are notably different than in non-polar solvents, and a single OH stretching mode is observed at 3543 and 3536 cm^{-1}, respectively (Table 4). Interestingly, the IR spectra of phenol in benzene and toluene show a single OH stretching mode at 3556 and 3550 cm^{-1}, respectively.[44,49] These studies and others[50] have shown computational evidence for the phenol-benzene/toluene dimers having a T-shaped geometry and OH···π and CH···π interactions. It was thus expected that similar interactions for **oPP** in these aromatic solvents would be present. Minimization of **PP2** and **PP3** isomers (the two **oPP** isomers having OH directed away from the P atom) with benzene did indeed afford two very similar T-shaped dimers differing by only 0.2 kcal/mol. The NCI plots show green (attractive) surfaces for the two types of OH···π and CH···π interactions.

Applications of counterpoise corrections for Basis Set Superposition Error (BSSE) allowed estimation of complexation energies of −6.1 kcal/mol, which are close in agreement with those values determined for phenol-benzene dimer (−4.9 kcal/mol).[51] The observed OH frequency at 3543 cm^{-1} compares most favorably with the anharmonic OH frequency of 3545 cm^{-1} for the lower energy **PP3**···benzene dimer, and is only off by 23 cm^{-1} from the value calculated for the **PP2**···benzene adduct. ^{31}P NMR shift calculations on the **PP2** and **PP3** adducts of benzene yield −121.1 and −178.7 ppm, respectively, which if averaged (−149.9), are near the observed value of −153.6 ppm in benzene. It is thus likely some mixture of these two **oPP** adducts with benzene is present in this solvent.

By analogy to past studies on phenol, it is very likely that **oPP** has significant associations with other solvents such as dichloromethane. These numerous possibilities, however, were not investigated further in this study. There is yet another different phenomenon worth examining in regards to the IR data obtained in the non-polar solvents. Since phenol and its related derivatives have shown self-aggregation behavior in solution, usually at higher concentrations, we have thus undertaken preliminary studies of possible dimers (and trimers) of **oPP**. In order to limit this line of inquiry, attention was directed to selected examples having the OH group directed away from the phosphorus atom so as to maximize opportunities for intermolecular OH···P and OH···π interactions (Table 6).

The X-ray structure of **oPP** revealed **PP2** monomers bridged by intermolecular OH···P hydrogen bonding (*vide supra*). Subjecting a hypothetical pair of these **PP2** units to full minimization (B3LYP-D3(BJ)/6-311++G(d,p) results in the dimer undergoing reorganizing to a stacked dimer with OH···P bonds, as shown in Table 7. In this dimer, some lesser degree of P···HO hydrogen bonding (non-linear) is retained, but in return adds π-π stacking interactions as well as additional OH···π interactions. Using the **PP2**–**PP2** dimer as a starting geometry, but rotating one of the PC bonds so as to establish an initial **PP2**–**PP3** dimer, followed by minimization leads to a comparable structure that is 0.3 kcal/mol different in total energy. Both

Research Article
doi.org/10.1002/ejic.202400260

Table 6. Computed structures with overlayed NCI plots, calculated energies for **oPP**-solvent dimers, and computed IR data B3LYP-D3(BJ)/6-311 + + G(d,p)// B3LYP-D3(BJ)/6-311 + + G(d,p)).

	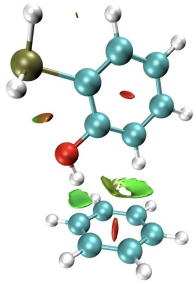 PP2-Benzene	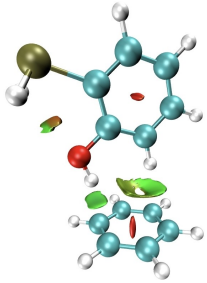 PP3-Benzene
complexation energy (corrected, kcal/mol)	−6.11	−6.09
IR (OH Modes, anharmonic, cm^{-1})	3521.6	3544.8
IR (PH_2 Modes, anharmonic, cm^{-1})	2298.2, 2261.0	2293.8, 2290.1

Table 7. Computed structures with overlayed NCI plots, calculated energies for **oPP-oPP** dimers, and computed IR data B3LYP-D3(BJ)/6-311 + + G(d,p)// B3LYP-D3(BJ)/6-311 + + G(d,p)).

	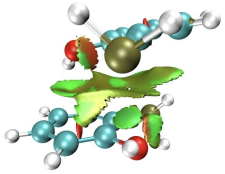 **PP2–PP3**	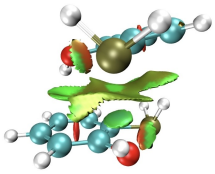 **PP2–PP2**	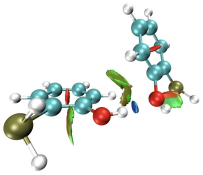 **PP3–PP4**	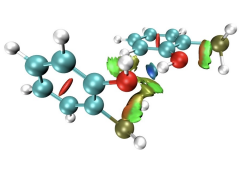 **PP3–PP3**
complexation energy (corrected, kcal/mol)	−12.10	−12.41	−7.86	−8.48
IR (OH Modes, anharmonic, cm^{-1})	3586.1, 3522.3	3580.2, 3480.9	3556.7, 3474.1	3635.7, 3486.6
IR (PH_2 Modes, anharmonic, cm^{-1})	2311.8, 2314.9, 2294.2, 2280.4	2304.4,2311.7, 2316.5, 2290.3	2274.9, 2269.2, 2244.7, 2232.5	2304.5, 2309.4, 2286.1, 2286.5

structures show extensive regions of green surfaces in the NCI plots for the π-π interactions. Also visible are green discs for the weak OH···P **HB** present.

There is a delicate balance of forces dictating the structures of such dimers. Using the same (X-ray) starting geometry, but rotating the PC and/or OC bonds to represent potential **PP3**–**PP4** or **PP3**–**PP3** dimers, and again minimizing, leads to different types of dimers. The **PP3**–**PP4** dimer that is generated largely retains the original form of hydrogen bonding shown in the X-ray structure, but the **PP3**–**PP3** dimer favors OH···O(H) **HB** over OH···P **HB**. The **HB** in these two dimers is stronger than in the first two, as shown by the blue discs in the corresponding NCI plots. Counterpoise calculations with corrections for BSSE show complexation energies of −12.1 to −12.4 kcal/mol for **PP2**–**PP2** and **PP2**–**PP3** dimers, −7.9 kcal/mol for **PP3**–**PP4**, and −8.5 kcal/mol for **PP3**–**PP3** dimers. An exhaustive search for other possible dimers were not undertaken due to the rather large number of possible structures.

The predicted OH frequencies of 3586 and 3522 cm^{-1} for the **PP2**–**PP3** dimer fall within the 3506–3610 cm^{-1} observed in cyclohexane, thus based on IR data alone, one can not rule out the presence of **oPP** dimers in solution, either solely or in equilibrium with monomers **PP1**–**PP4**. Past studies of phenol would suggest that at the low concentrations used on the IR studies, aggregation should be minimal. In order to probe this question experimentally, we have undertaken studies of **oPP** in cyclohexane-d_{12} using diffusion ordered spectroscopy (DOSY).[52] This method can assess the number of species in solution, provided they are sufficiently different in size from one another. Diffusion coefficients for each species are also provided (see SI). This method often employs an external calibration curve so that the diffusion coefficients can be correlated into molecular weights for each species.[53] This methodology was used recently to assess intramolecular versus intermolecular **HB** in phosphoryl-containing secondary alkanols.[54] For our present purposes, as the measurement of diffusion coefficients is dependent on not only MW but also the hydrodynamic radii (ie, shape of the molecule), we chose to record DOSY NMR spectra with and without *o*-chlorotoluene (**oDCT**), which has essentially the same molecular weight and hydrodynamic profile as **oPP**. Such experiments revealed that **oPP** and **oDCT** have essentially the same diffusion coefficients in cyclohexane (< 1% difference), supporting the hypothesis that formation of dimers and higher self-aggregates in this solvent is minimal.

Research Article
doi.org/10.1002/ejic.202400260

Conclusions

Extensive theoretical calculations on the primary phosphine **oPP** have identified four low energy conformations **PP1**–**PP4** in the gas phase. The lowest energy isomer **PP4** features bifurcated dihydrogen bonding as ascertained by RDG and NCI plots. The isomer **PP1** features a weak intramolecular hydrogen bond. This finding is unusual in that **DHB** interactions, especially involving non-polar EH bonds, are often of lower energy than **HB** interactions, but in this particular case, a pair of **DHB** interactions is more favorable than a single **HB** interaction. In the solid state, the molecules of **oPP** are bridged by intermolecular P···HO **HB** as determined by single crystal X-ray diffraction studies. In solution, NMR and IR spectroscopic studies suggest that **oPP** behaves much like phenol in that OH···π **HB** dimers with aromatic solvents such as benzene occur. Significant changes in the ^{31}P NMR shifts of **oPP** with varying solvents can be correlated against solvatomagnetic β_1 parameters that quantify solvent hydrogen bond accepting capabilities. In non-polar solvents such as cyclohexane, **oPP** is monomeric as ascertained by ^{1}H DOSY NMR methods. Four OH modes are observed in non-polar solvents, which have been attributed to the four conformations **PP1**–**PP4** found by computational methods. Calculations of the anharmonic OH modes agrees in general with this assignment. Further definitive assignments to each isomer may require costlier higher level theoretical analyses and/or specialized experiments such as 2D IR spectroscopy or laser-induced IR spectroscopy, such as has been used for studies of *o*-cresol that show rather strong solvent dependency for the UV-visible spectra.[50,55]

Acknowledgements

We thank the National Science Foundation (CHE #1955845 & CHE #2246810) for support of this work. We also acknowledge Dr. Milan Gembicky (Department of Chemistry and Biochemistry, University of California, San Diego) for crystallographic assistance and Dr. Joshua R. Gaffen for helpful discussions.

Conflict of Interests

The authors declare no conflict of interest.

Data Availability Statement

The data that support the findings of this study are available in the supplementary material of this article. Crystallographic information for **oPP** has been deposited with the Cambridge Crystallographic Database (CCDC # 2351201).

Keywords: Organophosphorus · hydrogen bonding · dihydrogen bonding · NMR spectroscopy · IR spectroscopy

[1] G. Gilli, P. Gilli, *The Nature of the Hydrogen Bond: Outline of a Comprehensive Hydrogen Bond Theory*, IUCr Monographs on Crystallography (23), Oxford University Press, Oxford UK, **2009**.
[2] S. J. Grabowski, *J. Phys. Org. Chem.* **2013**, *26*(6), 452–459.
[3] a) R. H. Crabtree, *Chem. Soc. Rev.* **2017**, *46*(6), 1720–1729; b) X. Chen, J.-C. Zhao, S. G. Shore, *Acct. Chem. Res.* **2013**, *46*(11), 2666–2675.
[4] G. A. Landrum, N. Goldberg, R. Hoffmann, R. M. Minyaev, *New J. Chem.* **1998**, *22*, 883–890.
[5] R. Custelcean, J. E. Jackson, *Chem. Rev.* **2001**, *101*, 1963–1980.
[6] N. V. Belkova, E. S. Shubina, L. M. Epstein, *Acc. Chem. Res.* **2005**, *38*, 624–631.
[7] V. I. Bakhmutov, *Dihydrogen Bonds: Principles, Experiments, and Applications*, John Wiley & Sons, Inc. **2008**. DOI: 10.1002/9780470226759.ch9.
[8] S. J. Grabowski, J. Leszczynski, *Dihydrogen Bonds: Novel Feature of Hydrogen Bond Interactions. In Practical Aspects of Computational Chemistry, Methods, Concepts and Applications*, (Eds: J. Leszczynski, M. K. Shukla), Springer, Dororecht, **2009**.
[9] a) D. W. Stephan, *J. Am. Chem. Soc.* **2015**, *137*(32), 10018–10032; b) D. W. Stephan, G. Erker, *Angew. Chem. Int. Ed.* **2015**, *54*(22), 6400–6441; c) D. W. Stephan, *J. Am. Chem. Soc.* **2021**, *143*(48), 20002–20014.
[10] a) G. E. Arnott, P. Moquist, C. G. Daniliuc, G. Kehr, G. Erker, *J. Inorg. Chem.* **2014**, *2014*(8), 1394–1398; b) L. Greb, C. G. Daniliuc, K. Bergander, J. Paradies, *Angew. Chem. Int. Ed. Engl.* **2013**, *52*(22), 5876–5879; c) Z. Mo, E. L. Kolychev, A. Rit, J. Campos, H. Niu, S. Aldridge, *J. Am. Chem. Soc.* **2015**, *137*(38), 12227–12230.
[11] a) S. Grimme, H. Kruse, L. Goerigk, G. Erker, *Angew. Chem. Int. Ed. Engl.* **2010**, *49*(8), 1402–1405; b) G. Skara, F. De Vleeschouwer, P. Geerlings, F. De Proft, B. Pinter, *Sci. Rep.* **2017**, *7*(1), 16024; c) L. Liu, L. L. Cao, Y. Shao, G. M. Ménard, D. W. Stephan, *Chem.* **2017**, *3*, 259–267.
[12] F. Kutter, E. Lork, S. Mebs, J. Beckmann, *Organometallics* **2018**, *37*(22), 4287–4296.
[13] J. W. Heinicke, *Chemistry* **2023**, *30*(6), e202302740.
[14] K. Issleib, R. Vollmer, *Z. Chem.* **1978**, *18*(12), 451–452.
[15] J. Heinicke, A. Tzschach, *Z. Chem.* **1980**, *20*(9), 342–343.
[16] a) L. J. Higham, *Catal. Met. Complexes* **2011**, *37*, 1–19; b) B. Stewart, A. Harriman, L. J. Higham, *Organometallics* **2011**, *30*(20), 5338–5343; c) J. T. Fleming, L. J. Higham, *Coord. Chem. Rev.* **2015**, *297–298*, 127–145.
[17] a) F. Horky, R. Franz, C. Bruhn, R. Pietschnig, *Chem. Eur. J.* **2023**, *29*(68), e202302518; b) F. Horký, C. Bruhn, D. Kargin, R. Pietschnig, *Adv. Syn. Cat.* **2024**, *366*, 3354–3360; c) F. Horky, C. Bruhn, R. Pietschnig, *Eur. J. Inorg. Chem.* **2024**, *accepted*, DOI: 10.1002/ejic.202400439; d) M. Brynda, *Coord. Chem. Rev.* **2005**, *249*(19–20), 2013–2034.
[18] a) M. P. Washington, V. B. Gudimetla, F. L. Laughlin, N. Deligonul, S. He, J. L. Payton, M. C. Simpson, J. D. Protasiewicz, *J. Am. Chem. Soc.* **2010**, *132*(13), 4566–4567; b) M. P. Washington, J. L. Payton, M. C. Simpson, J. D. Protasiewicz, *Organometallics* **2011**, *30*(7), 1975–1983; c) F. L. Laughlin, A. L. Rheingold, N. Deligonul, B. J. Laughlin, R. C. Smith, L. J. Higham, J. D. Protasiewicz, *Dalton Trans.* **2012**, *41*(39), 12016–12022; d) F. L. Laughlin, N. Deligonul, A. L. Rheingold, J. A. Golen, B. J. Laughlin, R. C. Smith, J. D. Protasiewicz, *Organometallics* **2013**, *32*(23), 7116–7121; e) M. C. Simpson, J. D. Protasiewicz, *Pure Appl. Chem.* **2013**, *85*(4), 801–815; f) S. Wu, N. Deligonal, J. D. Protasiewicz, *Dalton Trans.* **2013**, *42*(41), 14866–14874; g) S. Wu, A. L. Rheingold, J. D. Protasiewicz, *Chem. Commun.* **2014**, *50*(75), 11036–11038.
[19] L. Nyulászi, D. Szieberth, G. I. Csonka, J. Réffy, J. Heinicke, T. Veszprémi, *Struct. Chem.* **1995**, *6*, 1–7.
[20] H.-G. Korth, M. I. d. Heer, *J. Phys. Chem. A* **2002**, *106*(37), 8779–8789.
[21] A. M. Stone, A. L. Rheingold, J. D Protasiewicz. Manuscript in preparation.
[22] W. Wang, Y. Zhang, K. Huang, *Chem. Phys. Lett.* **2005**, *411*(4), 439–444.
[23] A. N. Isaev, *Comput. Theor. Chem.* **2018**, *1142*, 28–38.
[24] N. Mardirossian, M. Head-Gordon, *J. Chem. Phys.* **2016**, *144*(21), 214110.
[25] J. Heinicke, R. Kadyrov, M. K. Kindermam, M. Koesling, P. G. Jones, *Chem. Ber.* **1996**, *129*(12), 1547–1560.
[26] a) R. F. W. Bader, *Atoms in Molecules. A Quantum Theory*, International Series of Monographs on Chemistry (22), Cambridge University Press, Cambridge, UK, **1991**; b) R. F. W. Bader, *Chem. Rev.* **1991**, *91*(5), 893–928.
[27] E. R. Johnson, S. Keinan, P. Mori-Sánchez, J. Contreras-García, A. J. Cohen, W. Yang, *J. Am. Chem. Soc.* **2010**, *132*(18), 6498–6506.
[28] a) T. Lu, F. Chen, *J. Comput. Chem.* **2012**, *33*(5), 580–592; b) AIMAll (Version 19.10.12); TK Gristmill Software: Overland Park KS, USA, 2019. aim.tkgristmill.com; c) W. Humphrey, A. Dalke, K. Schulten, *J. Mol. Graphics* **1996**, *14*(1), 33–38; d) T. Lu, Q. Chen, Visualization Analysis of Weak Interactions in Chemical Systems. In Comprehensive *Computa-*

tional Chemistry (Eds: M. Yáñez, Boyd R. J.) First Edition, Elsevier **2024**, pp. 240–264.
[29] a) C. R. Wick, T. Clark, *J. Mol. Mod.* **2018**, *24*(6), 142; b) S. Shahbazian, *Chemistry* **2018**, *24*(21), 5401–5405.
[30] J. R. Lane, J. Contreras-Garcia, J. P. Piquemal, B. J. Miller, H. G. Kjaergaard, *J. Chem. Theory Comput.* **2013**, *9*(8), 3263–3266.
[31] NBO Version 3.1, E. D. Glendening, A. E. Reed, J. E. Carpenter, F. Weinhold.
[32] L. Yang, T. A. Hubbard, S. L. Cockroft, *Chem. Commun.* **2014**, *50*(40), 5212–5214.
[33] a) H. Ishikawa, T. Kawasaki, R. Inomata, *J. Phys. Chem. A* **2015**, *119*(4), 601–609; b) H. Ishikawa, A. Saito, M. Sugiyama, N. Mikami, *J. Chem. Phys.* **2005**, *123*(22), 224309; c) E. D. Voronova, I. E. Golub, A. A. Pavlov, N. V. Belkova, O. A. Filippov, L. M. Epstein, E. S. Shubina, *Chem. Asian J.* **2018**, *13*(20), 3084–3089.
[34] M. Ghalib, P. G. Jones, S. Lysenko, J. W. Heinicke, *Organometallics* **2014**, *33*(3), 804–816.
[35] N. B. Jones, C. H. Sharp, D. Troya, J. R. Morris, *J. Phys. Chem. Lett.* **2021**, *12*(20), 4987–4992.
[36] S. Gholami, M. Aarabi, S. J. Grabowski, *ChemPhysChem* **2024**, *25*(4), e202300849.
[37] a) S. A. Buckler, M. Epstein, *Tetrahedron* **1962**, *18*(11), 1211–1219; b) S. A. Buckler, V. P. Wystrach, *J. Am. Chem. Soc.* **1961**, *83*(1), 168–173.
[38] a) C. Laurence, S. Mansour, D. Vuluga, A. Planchat, J. Legros, *J. Org. Chem.* **2021**, *86*(5), 4143–4158; b) C. Laurence, J. Legros, P. Nicolet, D. Vuluga, A. Chantzis, D. Jacquemin, *J. Phys. Chem. B* **2014**, *118*(27), 7594–7608; c) C. Laurence, J. Legros, A. Chantzis, A. Planchat, D. Jacquemin, *J. Phys. Chem. B* **2015**, *119*(7), 3174–3184.
[39] S. K. Latypov, F. M. Polyancev, D. G. Yakhvarov, O. G. Sinyashin, *Phys. Chem. Chem. Phys.* **2015**, *17*(10), 6976–6987.
[40] a) L. B. Krivdin, *Magn. Reson. Chem.* **2020**, *58*(6), 478–499; b) I. G. Shenderovich, *Methods* **2020**, *1*(1), 61–70.
[41] J. Tomasi, B. Mennucci, R. Cammi, *Chem. Rev.* **2005**, *105*(8), 2999–3093.
[42] W. H. Hersh, T. Y. Chan, *Beilstein J. Org. Chem.* **2023**, *19*, 36–56.
[43] a) M. A. Czarnecki, Y. Morisawa, Y. Katsumoto, T. Takaya, S. Singh, H. Sato, Y. Ozaki, *Phys. Chem. Chem. Phys.* **2021**, *23*(35), 19188–19194; b) A. M. Fedor, M. J. Toda, *J. Chem. Educ.* **2014**, *91*(12), 2191–2194; c) M. Kolar, P. Hobza, *J. Phys. Chem. A* **2007**, *111*(26), 5851–5854; d) S. K. Panja, S. Verma, S. Saha, *J. Mol. Struct.* **2019**, *1193*, 103–109; e) N. A. Seifert, A. L. Steber, J. L. Neill, C. Perez, D. P. Zaleski, B. H. Pate, A. Lesarri, *Phys. Chem. Chem. Phys.* **2013**, *15*(27), 11468–11477.
[44] a) L. Cesari, L. Canabady-Rochelle, F. Mutelet, *Struct. Chem.* **2018**, *29*(1), 179–194; b) X. Yuan, D. Zheng, X. Wang, P. Liu, J. Ma, *J. Phys. Chem. A* **2016**, *120*(51), 10196–10206; c) D. Zheng, X. A. Yuan, H. Ma, X. Li, X. Wang, Z. Liu, J. Ma, *R. Soc. Open Sci.* **2018**, *5*(3), 171928.
[45] J. C. Zapata Trujillo, L. K. McKemmish, *J. Phys. Chem. A* **2023**, *127*(7), 1715–1735.
[46] J. C. Z. Trujillo, A.-M. Syme, K. N. Rowell, B. P. Burns, E. S. Clark, M. N. Gorman, L. S. D. Jacob, P. Kapodistrias, D. J. Kedziora, F. A. R. Lempriere, et al., *Front. Astron. Space Sci.* **2021**, *8*(8), 639068.
[47] a) V. Barone, *J. Chem. Phys.* **2005**, *122*(014108), 014101–014110; b) T. Fornaro, M. Biczysko, S. Monti, V. Barone, *Phys. Chem. Chem. Phys.* **2014**, *16*(21), 10112–10128.
[48] M. W. D. Hanson-Heine, *J. Phys. Chem. A* **2019**, *123*(45), 9800–9808.
[49] M. Saggu, N. M. Levinson, S. G. Boxer, *J. Am. Chem. Soc.* **2011**, *133*(43), 17414–17419.
[50] L. Cesari, L. Canabady-Rochelle, F. Mutelet, *Struct. Chem.* **2018**, *29*(1), 179–194.
[51] P. P. Zhou, X. Yang, D. G. Zhou, S. Liu, *Theor. Chem. Acc.* **2016**, *135*(100), 1–11.
[52] a) K. F. Morris, S. Charles, *J. Am. Chem. Soc.* **1992**, *114*(8), 3139–3141; b) Y. Cohen, L. Avram, L. Frish, *Angew. Chem., Int. Ed.* **2005**, *44*(4), 520–554; c) D. Li, G. Kagan, R. Hopson, P. G. Williard, *J. Am. Chem. Soc.* **2009**, *131*(15), 5627–5634.
[53] R. Neufeld, D. Stalke, *Chem. Sci.* **2015**, *6*(6), 3354–3364.
[54] M. P. Pasechnik, A. G. Matveeva, K. A. Lyssenko, R. R. Aysin, A. F. Smol'yakov, Y. V. Zubavichus, I. A. Godovikov, E. I. Goryunov, *J. Mol. Struct.* **2019**, *1175*, 874–881.
[55] a) C. Trindle, *J. Phys. Chem. A* **2000**, *104*(22), 5298–5301; b) A. Welzel, A. Hellweg, I. Merke, W. Stahl, *J. Mol. Spectrosc.* **2002**, *215*(1), 58–65; c) X. Yuan, D. Zheng, X. Wang, P. Liu, J. Ma, *J. Phys. Chem. A* **2016**, *120*(51), 10196–10206; d) D. Zheng, X. A. Yuan, H. Ma, X. Li, X. Wang, Z. Liu, J. Ma, *R. Soc. Open Sci.* **2018**, *5*(3), 171928.

Manuscript received: April 30, 2024
Revised manuscript received: June 7, 2024
Accepted manuscript online: June 21, 2024
Version of record online: September 3, 2024